



# *Contributions of greenhouse gas forcing and the Southern Annular Mode to historical Southern Ocean surface temperature trends*

Article

Published Version

Kostov, Y., Ferreira, D., Marshall, J. and Armour, K. (2018) Contributions of greenhouse gas forcing and the Southern Annular Mode to historical Southern Ocean surface temperature trends. *Geophysical Research Letters*, 45 (2). pp. 1086-1097. ISSN 0094-8276 doi: <https://doi.org/10.1002/2017GL074964> Available at <http://centaur.reading.ac.uk/74921/>

It is advisable to refer to the publisher's version if you intend to cite from the work.

To link to this article DOI: <http://dx.doi.org/10.1002/2017GL074964>

Publisher: American Geophysical Union

All outputs in CentAUR are protected by Intellectual Property Rights law, including copyright law. Copyright and IPR is retained by the creators or other copyright holders. Terms and conditions for use of this material are defined in the [End User Agreement](#).

[www.reading.ac.uk/centaur](http://www.reading.ac.uk/centaur)

**CentAUR**

Central Archive at the University of Reading

Reading's research outputs online

## RESEARCH LETTER

10.1002/2017GL074964

## Key Points:

- CMIP5 models have diverse Southern Ocean SST response functions to SAM and greenhouse gas forcing
- Weak warming (strong cooling) responses to greenhouse gas forcing (SAM) favor multidecadal Southern Ocean cooling
- Biases in the simulated SAM trends strongly affect the models' historical Southern Ocean SST trends

## Supporting Information:

- Supporting Information S1

## Correspondence to:

Y. Kostov,  
yavor.kostov@physics.ox.ac.uk

## Citation:

Kostov, Y., Ferreira, D., Armour, K. C., & Marshall, J. (2018). Contributions of greenhouse gas forcing and the Southern Annular Mode to historical Southern Ocean surface temperature trends. *Geophysical Research Letters*, 45. <https://doi.org/10.1002/2017GL074964>

Received 18 JUL 2017

Accepted 2 JAN 2018

Accepted article online 8 JAN 2018

## Contributions of Greenhouse Gas Forcing and the Southern Annular Mode to Historical Southern Ocean Surface Temperature Trends

Yavor Kostov<sup>1</sup>, David Ferreira<sup>2</sup>, Kyle C. Armour<sup>3</sup>, and John Marshall<sup>4</sup>

<sup>1</sup>Department of Physics, University of Oxford, Oxford, UK, <sup>2</sup>Department of Meteorology, University of Reading, Reading, UK, <sup>3</sup>School of Oceanography and Department of Atmospheric Sciences, University of Washington, Seattle, WA, USA, <sup>4</sup>Department of Earth, Atmospheric, and Planetary Sciences, Massachusetts Institute of Technology, Cambridge, MA, USA

**Abstract** We examine the 1979–2014 Southern Ocean (SO) sea surface temperature (SST) trends simulated in an ensemble of coupled general circulation models and evaluate possible causes of the models' inability to reproduce the observed 1979–2014 SO cooling. For each model we estimate the response of SO SST to step changes in greenhouse gas (GHG) forcing and in the seasonal indices of the Southern Annular Mode (SAM). Using these step-response functions, we skillfully reconstruct the models' 1979–2014 SO SST trends. Consistent with the seasonal signature of the Antarctic ozone hole and the seasonality of SO stratification, the summer and fall SAM exert a large impact on the simulated SO SST trends. We further identify conditions that favor multidecadal SO cooling: (1) a weak SO warming response to GHG forcing, (2) a strong multidecadal SO cooling response to a positive SAM trend, and (3) a historical SAM trend as strong as in observations.

### 1. Introduction

Unlike the rapidly warming Arctic, the Southern Ocean (SO) exhibited a notable multidecadal cooling trend from the beginning of the satellite record in 1979 through 2014 (Figure 1a; see also Armour & Bitz, 2015; Armour et al., 2016; Fan et al., 2014; Jones et al., 2016). Most historical simulations with state-of-the-art coupled models participating in the Climate Modeling Intercomparison Project phase 5 (CMIP5) do not reproduce the negative SO sea surface temperature (SST) trends and instead show gradual warming around Antarctica (Figure 1b). Moreover, the intermodel spread in simulated SO SST trends within the CMIP5 ensemble is large and comparable to the difference between the ensemble mean and the observations (Figure S1 of the supporting information). In this study we attempt to evaluate the mechanisms governing the 1979–2014 SO SST trends in CMIP5 historical simulations and interpret both the intermodel diversity and the SO warming bias relative to observations.

Marshall et al. (2015) relate the observed Antarctic-Arctic warming asymmetry under greenhouse gas (GHG) forcing to the meridional overturning circulation advecting the heat anomaly in the upper ocean northward like a passive tracer. The Southern Ocean is a region where the background circulation upwells deep water masses unmodified by GHG forcing and dampens the warming rate at the surface (Armour et al., 2016; Marshall et al., 2015). CMIP5 experiments unanimously show a gradual positive SO SST response to GHG forcing, but they disagree on the magnitude of this regional response with some models warming much faster than others (Marshall et al., 2014).

In addition to GHG forcing, stratospheric ozone depletion and unforced atmospheric variability are also potential drivers of historical SO SST trends. The observed 1979–2014 SO cooling took place during a period of poleward intensification of the Southern Hemisphere westerly winds, as reflected in the tendency toward a more positive Southern Annular Mode (SAM) index (Thompson et al., 2011) (see also Figure 1c). Consistent with the seasonal signature of the Antarctic ozone hole, the strongest positive trend in the 1979–2014 SAM index is observed during the austral summer and fall: December–May (Figure 1c). It is noteworthy that there is uncertainty in the magnitude of the historical SAM trend (Swart et al., 2015). Here we consider two different data sets that provide distinct estimates of the observed SAM trend (Figure 1c): the HadSLP2r gridded observations (Allan & Ansell, 2006) and the ERA-Interim reanalysis (Dee et al., 2011).

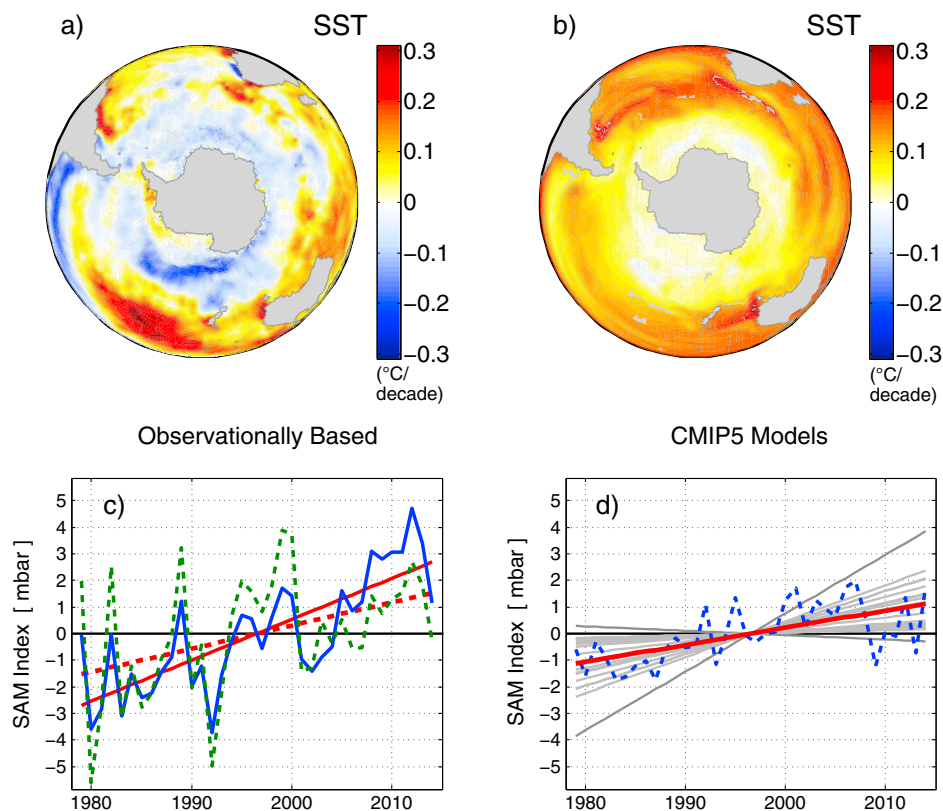


**Figure 1.** (a) Observed SST trends ( $^{\circ}$  C per decade) for the 1979–2014 period based on the HadISST data set; (b) simulated SST trends ( $^{\circ}$  C per decade) for the 1979–2014 period: an ensemble mean of 19 CMIP5 historical experiments extended under the RCP8.5 scenario; (c) observationally based time series from HadSLP2r (blue, solid) and ERA-Interim (green, dashed) of the December–May SAM index (mbar). Straight lines show the linear trends; and (d) same as Figure 1c but based on the CMIP5 simulations: ensemble mean (blue), ensemble mean trend (red), and all individual model trends (gray).

There is also substantial disagreement among the SAM trends simulated by models (Thomas et al., 2015) and large differences between CMIP5 models and the observationally constrained products (Figures 1c and 1d). A subset of CMIP5 historical simulations overestimates the observed trend in the SAM. In contrast, other CMIP5 models underestimate both the HadSLP2r and the ERA-Interim SAM trend (Figures 1c and 1d). Negative biases in the simulated SAM trends may be attributed to equatorward biases in the climatological position of the Southern Hemisphere surface jet across CMIP5 (Bracegirdle et al., 2013). The earlier generation of CMIP3 models exhibited a similar bias in the location of the Southern Hemisphere zonal wind stress maximum (Sen Gupta et al., 2009). CMIP models are also prone to underestimating the historical rate of stratospheric ozone depletion (Neely et al., 2014), which projects onto the seasonal SAM anomalies.

Is there a causal connection between a given model's failure to reproduce the magnitude of the positive SAM trend and its SO warming bias relative to observations? Models and observations show that a strengthening and a poleward shift of the westerly winds induce, within weeks, a negative SST response around Antarctica (Ciaсто & Thompson, 2008; Fyfe et al., 2007; Hall & Visbeck, 2002; Marshall et al., 2014; Purich et al., 2016; Russell et al., 2006). This fast cooling response to SAM is influenced by anomalous northward Ekman drift of colder water (Ferreira et al., 2015; Kostov et al., 2017), but some models suggest that anomalous air-sea heat fluxes also play an important role (Oke & England, 2004). Overall, coupled general circulation models (GCMs) consistently show a negative SST response to SAM on time scales shorter than 2 years (Kostov et al., 2017).

However, the SO SST in many GCMs does not respond monotonically to a step increase in the SAM index but instead exhibits a two-time scale response: the fast SO SST cooling is followed by gradual warming (Ferreira et al., 2015; Kostov et al., 2017). The slow response involves a more complicated mechanism: SAM-induced Ekman upwelling (Bitz & Polvani, 2012), partially compensated by eddy transport, gives rise to subsurface warming that is in turn communicated to the mixed layer on longer time scales (Ferreira et al., 2015). The time

scale of transition between the fast (cooling) and the slow (warming) response to a step change in the SAM varies considerably across CMIP5 models, and several step-response functions do not cross over to a positive SO SST response at all. Ferreira et al. (2015) find that the transition from initial cooling to long-term warming in the step-response functions is model dependent and can be explained in terms of the background ocean temperature gradients on which the anomalous wind-induced circulation acts. In turn, Kostov et al. (2017) relate the intermodel diversity in the fast and slow SO SST responses to biases in the horizontal and vertical temperature gradients in the models' SO climatology. Eddy compensation and air-sea heat fluxes likely also affect the slow response to SAM and contribute to the intermodel spread.

Here we use linear convolution theory (Hasselmann et al., 1993) to demonstrate that differences in the GCMs' inherent SO SST responses to the seasonal SAM indices and GHG forcing affect the models' ability to reproduce the 1979–2014 SO SST cooling. We also examine how biases in the simulation of SAM trends affect the evolution of SO SST anomalies in CMIP5 historical experiments. We focus particularly on the December–May seasonal SAM as that is the period of the year when stratospheric ozone depletion most strongly affects the atmospheric circulation near the surface. We explicitly do not consider any drivers of SO SST changes other than GHG forcing and SAM. Our analysis accounts for the impact of freshwater flux anomalies on stratification and SSTs but only to the extent that this is associated with changes in the hydrological cycle induced by GHG forcing or SAM trends. We thus test the hypothesis that the December–May SAM along with GHG forcing can explain a large fraction of the intermodel differences in SO SST trends across CMIP5 historical simulations. Understanding the diversity of model behavior helps shed light on the physical mechanisms driving the SO SST trends, as well as on possible reasons why CMIP5 models have been unable to capture the observed changes.

## 2. Data and Methods

We consider four sets of numerical experiments performed with an ensemble of 19 CMIP5 models: preindustrial (PI) control simulations, abrupt CO<sub>2</sub> quadrupling experiments, historical simulations, and their extension under the RCP8.5 emission scenario (Taylor et al., 2012). For all models, we analyze the first ensemble member of the PI control simulations (r1i1p1). We regrid all GCM output to the same regular latitude-longitude grid, and for each time series we remove the long-term linear drift of the corresponding PI control simulations. We focus on the impact of GHG forcing and SAM on the historical evolution of SO SST defined as the area-weighted average of the SST between 55° S and 70° S. We first estimate each model's SO SST response function to a step change in the SAM (a step-response function) using the relationships between SST and SAM found in the unforced PI control simulations. We then estimate each model's SO SST step-response function to GHG forcing from the abrupt CO<sub>2</sub> quadrupling simulations. Using these step-response functions, we reconstruct the models' simulated historical SO SST trends and compare them to observations. Our reconstructions explain roughly half of the intermodel spread and thus highlight the important contribution of GHG forcing and SAM trends to the simulated SO SST trends. Correcting for biases in the models' seasonal SAM trends, we explore how the simulated SO SST would evolve if each model had reproduced a realistic SAM trend. Finally, we determine a subset of model-based SO SST step-response functions to GHG forcing and SAM that favor multidecadal SO SST cooling comparable to observations.

### 2.1. Estimating the Response of SO SST to SAM

We consider the impact of seasonal SAM changes on the SO SST, where we divide the year into two periods: December–May and June–November. For each CMIP5 PI control simulation and for each of the two seasonal periods, we calculate a SAM index (mbar) defined as the difference between the zonally averaged sea level pressure (SLP) at 40° S and 65° S, as in Swart et al. (2015). Positive values of the SAM index indicate a strengthening and/or a poleward shift of the westerly winds.

Following Kostov et al. (2017), we perform a multiple linear least squares regression of each model's annually averaged SO SST against the lagged seasonal SAM index to estimate the SO SST step-response function,  $SST_{\text{StepSAM}}(\tau, i)$  (°C/mbar) (see description in Text S1 in the supporting information and Kostov et al., 2017).  $SST_{\text{StepSAM}}(\tau, i)$  represents the transient adjustment of the SO SST to a step increase of the SAM in season  $i$ , where  $\tau$  is the time (years) since the step change.

We repeat the same procedure separately for the December–May and the June–November seasons. The step-response functions to December–May SAM are shown in Figure 2a and the responses to June–November

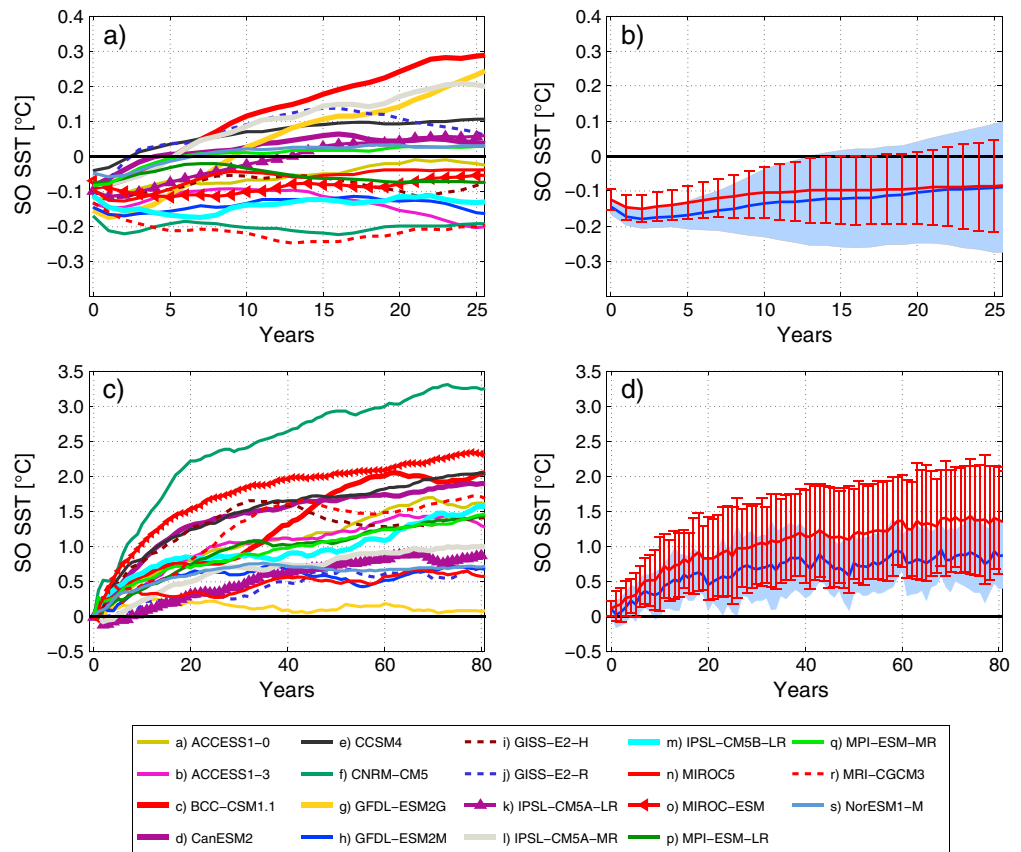


**Figure 2.** Left: Response functions of the annually averaged SO SST (55° S to 70° S) in CIMP5 models to a 1 standard deviation step increase in the (a) December–May SAM index and to an (c) abrupt CO<sub>2</sub> quadrupling (smoothed with a 20 year running mean). Different colors and line styles indicate individual model responses; right: Subset of the step-response functions to (b) SAM and (d) GHG forcing that favor multidecadal SO cooling (section 3.2) induced by the observed SAM trend as estimated from ERA-Interim (blue) and HadSLP2r (red) data. The thick blue/red lines show the mean response of the subset. Blue shading/red bars show one standard deviation for each subset.

SAM in Figure S2 in the supporting information. Consistent with Kostov et al. (2017), we find a large range of time scales on which the SO SST response to abrupt SAM changes crosses over from cooling to warming within CIMP5 models (Figure 2a). The SO SST step responses to SAM are not sensitive to the definition of the SAM index. Similar step-response functions are found using a SAM index defined as the first principal component of SLP south of 20° S (Text S2 and Figure S3), a metric that better reflects the geographic pattern associated with SAM variability (Haumann et al., 2014; Holland et al., 2017; Yeo & Kim, 2015).

We then consider CIMP5 historical simulations extended under the RCP8.5 emission scenario. For each model, we use the corresponding step-response function to estimate the contribution of SAM variability to the simulated 1979–2014 SO SST anomalies, denoted as  $\widehat{SST}_{\text{HistSAM}}(t)$  (° C). Following the methodology of Marshall et al. (2014), we convolve the seasonal step-response functions  $SST_{\text{StepSAM}}(\tau, i)$  (Figure 2a) with the 1979–2014 seasonal SAM,  $SAM_{\text{Hist}}(t, i)$  (mbar) (see details of the method and a full nomenclature in the supporting information). We therefore express  $\widehat{SST}_{\text{HistSAM}}(t)$  as

$$\widehat{SST}_{\text{HistSAM}}(t) \approx \sum_i \int_{t-\tau_{\text{max}}}^t SST_{\text{StepSAM}}(t-t', i) \left. \frac{dSAM_{\text{Hist}}(t', i)}{dt} \right|_{t'} dt', \quad (1)$$

where  $\tau_{\text{max}}$  is an imposed maximum cut-off lag. We assume a constant linear trend in the SAM,  $\frac{dSAM_{\text{Hist}}(t', i)}{dt}$  for each season  $i$ , but our results do not change substantially if we use the fully time varying  $SAM_{\text{Hist}}(t, i)$ . We then compute the linear trend in SO SST between 1979 and 2014, denoted as  $\widehat{SST}_{\text{TrendSAM}}$  (° C per decade). The latter represents an estimate for the SAM-induced component of the historical SO SST trend.

## 2.2. Estimating the Response of SO SST to GHG Forcing

SAM is not the only major driver of SO SST anomalies in historical simulations. Perturbations in the top-of-the-atmosphere (TOA) radiative forcing play an important role in climate change as modeled in the CMIP5 GCMs. The historical TOA radiative forcing has been overwhelmingly dominated by anthropogenic GHG emissions (Hansen et al., 2011). Major volcanic eruptions have exerted only an episodic cooling effect superimposed on the long-term warming trend (Hansen et al., 2011), and we do not account for them in our analysis. The local effect of aerosols and land use has been larger over the Northern Hemisphere. The nonlocal effect of anthropogenic aerosols and land use on Southern Ocean climate is thought to be relatively small (e.g., Xie et al., 2013), and thus, we neglect their impact on SO SST trends.

To obtain an estimate for the SO SST responses to a step change in GHG forcing, we consider CMIP5 experiments where CO<sub>2</sub> is abruptly quadrupled relative to PI values of ~280 ppm. We can think of the output from these idealized experiments as representing a range of plausible SO SST response functions to a step increase in GHG forcing, denoted  $SST_{4\times CO_2}(t)$ . For each model, we compute the SO SST anomalies from the abrupt quadrupling experiment (Figure 2c) relative to the PI control simulation from which the experiment was branched. The CMIP5 models show a large range of SO responses to CO<sub>2</sub> forcing with some models warming much faster than others. These step-response functions capture the combined effect of multiple mechanisms that set the SO response to GHG forcing, including changes in the heat and freshwater budgets and adjustments of the atmospheric circulation as represented in each model.

Thus, analogously to equation (1), the SO SST anomalies  $SST_{GHGhist}$  (°C) induced by the idealized trend in GHG forcing can be approximated as

$$\begin{aligned} \widehat{SST}_{GHGhist}(t) &= \int_0^t \frac{SST_{4\times CO_2}(t-t')}{F_{4\times CO_2}} \left. \frac{\partial F_{GHGhist}}{\partial t} \right|_{t'} dt' \\ &\approx \frac{F_{GHGtrend}}{F_{4\times CO_2}} \int_0^t SST_{4\times CO_2}(t-t') dt', \end{aligned} \quad (2)$$

where  $\partial F_{GHGhist}/\partial t = F_{GHGtrend}$  is the historical trend in greenhouse gas radiative forcing, and  $F_{4\times CO_2}$  is the radiative forcing corresponding to CO<sub>2</sub> quadrupling. As a simplification, we have assumed a linear increase in GHG forcing,  $F_{GHGtrend}$ , that corresponds to an exponential increase in the concentration of anthropogenic GHGs from a 280 ppm to a 480 ppm CO<sub>2</sub> equivalent over the course of 160 years between 1855 and 2014 (e.g., Hofmann et al. (2006) with updates and CO<sub>2</sub>-equivalent GHG metrics available at <https://www.esrl.noaa.gov/gmd/aggi/aggi.html>). We treat deviations from this trend as a contribution to the residual error in our analysis. Invoking the logarithmic dependence of radiative forcing on the CO<sub>2</sub>-equivalent concentration of well-mixed greenhouse gases, the factor  $F_{GHGtrend}/F_{4\times CO_2}$  is estimated to be

$$\frac{F_{GHGtrend}}{F_{4\times CO_2}} \approx \left( \frac{\ln(480) - \ln(280)}{\ln(4 \times 280) - \ln(280)} \right) \frac{1}{160 \text{ years}} \approx 2.43 \times 10^{-3} \left[ \frac{1}{\text{years}} \right]. \quad (3)$$

We then calculate the 1979–2014 linear trend in  $\widehat{SST}_{GHGhist}(t)$ , denoted by  $\widehat{SST}_{TrendGHG}$  (°C per decade), which represents the contribution of GHG forcing to the historical SO SST trend.

## 2.3. Reconstruction of SO SST Trends in Historical Simulations

We now consider the results of SAM and GHG convolutions to simultaneously account for both of these major drivers of historical SO SST anomalies. However, part of the historical trend in the SAM index is itself driven by GHG forcing (Kushner et al., 2001; Lee & Feldstein, 2013; Solomon & Polvani, 2016; Son et al., 2010; Wang et al., 2014). Thus, we cannot sum the SAM and GHG convolutions without subtracting an interaction term  $\widehat{SST}_{TrendInter}$ . This term represents the SST trend induced by the component of the SAM that is attributable to GHG forcing. We turn to the CMIP5 abrupt CO<sub>2</sub> quadrupling experiments to analyze the effect of GHG forcing on the SAM and to quantify  $\widehat{SST}_{TrendInter}$  (see section S3 and Figure S4 in the supporting information for a discussion of this approach). We estimate that over the recent historical period 1979–2014,  $\widehat{SST}_{TrendInter}$  is much smaller than  $\widehat{SST}_{TrendGHG}$  and  $\widehat{SST}_{TrendSAM}$ , the corresponding total GHG and total SAM contributions to the simulated SO SST trend.

Finally, we combine  $\widehat{SST}_{TrendSAM}$  and  $\widehat{SST}_{TrendGHG}$ , and we subtract the trend in the GHG-SAM interaction term  $\widehat{SST}_{TrendInter}$ . Hence, we obtain reconstructions of the 1979–2014 SO SST trend due to the combined effect of GHG forcing and SAM in the historical simulations:

$$\widehat{SST}_{TrendAll} = \widehat{SST}_{TrendSAM} + \widehat{SST}_{TrendGHG} - \widehat{SST}_{TrendInter}. \quad (4)$$

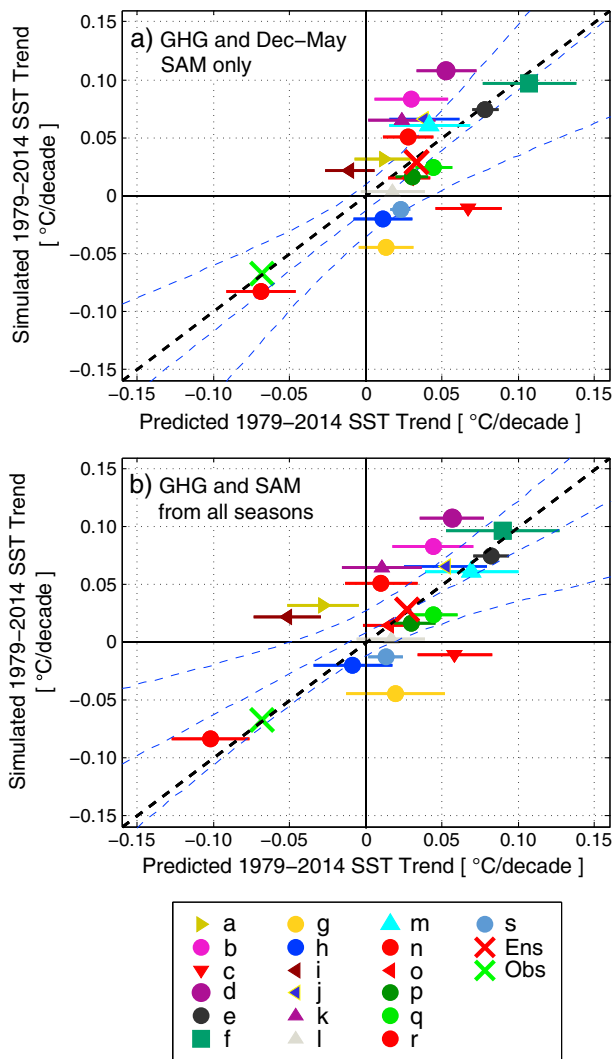


**Figure 3.** Comparison of the simulated 1979–2014 SO SST trends ( $^{\circ}\text{C}$  per decade) in CMIP5 historical experiments (vertical axis) against our reconstructions (equation (4), horizontal axis): (a) combining the contribution of GHG forcing and the summer/fall (December–May) SAM. (b) Same as in Figure 2a but including the contribution by the SAM in all seasons. Markers in Figures 3a and 3b represent individual models with the same color code and alphabetical legend as in Figures 2a and 2c. Horizontal bars show the  $1\sigma$  uncertainty on each reconstruction. A red cross denotes the ensemble mean of the simulations and reconstructions, and a green cross denotes the trend in the HadISST observations. Dashed blue lines denote a fitted regression line and the  $2\sigma$  confidence interval. The dashed black line denotes a one-to-one correspondence.

We also compute the corresponding uncertainties on each  $\widehat{\text{SST}}_{\text{TrendAll}}$  estimate (Text S4 in the supporting information).

Since the historical SAM trend is much stronger in the summer and fall compared to winter and spring, we consider two sets of reconstructions. In one reconstruction,  $\widehat{\text{SST}}_{\text{TrendSAM}}$  is estimated using the December–May SAM. In a second reconstruction, we consider the combined contribution of December–May and June–November SAM. We thus test the hypothesis that poleward intensification of the westerly winds in the austral summer and fall has exerted a particularly strong impact on the historical SO SST trends.

### 3. Results

#### 3.1. Historical SO SST Trends in CMIP5 Simulations

Our  $\widehat{\text{SST}}_{\text{TrendAll}}$  estimates using December–May SAM exhibit relatively good skill in recovering both the ensemble mean 1979–2014 SO SST trend and the behavior of individual GCMs (Figure 3a). This result demonstrates the important contribution of GHG forcing and SAM trends to the simulated SO SST trends. We find a strong correlation between our reconstructions and the actual SO SST trends in CMIP5 simulations ( $R = 0.67$ ). The slope of the weighted regression line is approximately 1.04 and highly significant ( $p < 0.001$ ). The weighted root-mean-square error (RMSE) for the ensemble of reconstructions is  $\sigma_{\text{RMSE}} = 0.031^{\circ}\text{C}$  per decade and is smaller than the intermodel standard deviation in 1979–2014 SO SST trends,  $0.050^{\circ}\text{C}$  per decade. Moreover, both the simulated and the reconstructed CMIP5 trends show a similar positive bias relative to the observed 1979–2014 SO SST trends from the Hadley Centre Sea Ice and Sea Surface Temperature (HadISST) data set (Rayner et al., 2003). Only one model (MRI-CGCM3) shows SO cooling comparable to observations. Similar results are obtained using an alternative definition of the SAM index as the first PC of SLP variability south of  $20^{\circ}\text{S}$  (Text S2 and Figure S5 in the supporting information).

The seasonality of the SAM impact is noteworthy. Including the contribution of winter-spring (June–November) SAM does not improve the reconstruction but introduces additional estimation errors and uncertainties (Figure 3b). Overall, the impact of summer-fall SAM on the SO SST trends is estimated to be much larger than the impact of winter-spring changes. This seasonality is consistent with the findings of Purich et al. (2016), who suggest that the SO SST is expected to show a stronger cooling response to a positive SAM trend in December–May compared to June–November. Moreover, our results are consistent with the seasonality of the Antarctic ozone hole whose impact on the SAM signal in the troposphere is most strongly manifested in the austral summer and fall (Gillett & Thompson, 2003; Solomon et al., 2015; Thompson & Solomon, 2002; Thompson et al., 2011). Henceforth, in our analysis and discussion we include only the December–May contribution to  $\widehat{\text{SST}}_{\text{TrendSAM}}$ .

Our reconstruction allows us to break down the simulated multidecadal SO SST trends into GHG and SAM contributions (Figure 4a). CMIP5 models agree that the GHG forcing contributes to warming around Antarctica over the 1979–2014 period, although the intermodel spread is large. In contrast, the sign of the December–May SAM contribution to the SST trends differs across models. In many of the CMIP5 GCMs, positive 1979–2014 seasonal SAM tendencies would induce SO cooling anomalies. However, as discussed in Kostov et al. (2017), several CMIP5 models such as CCSM4 are expected to simulate multidecadal SO warming



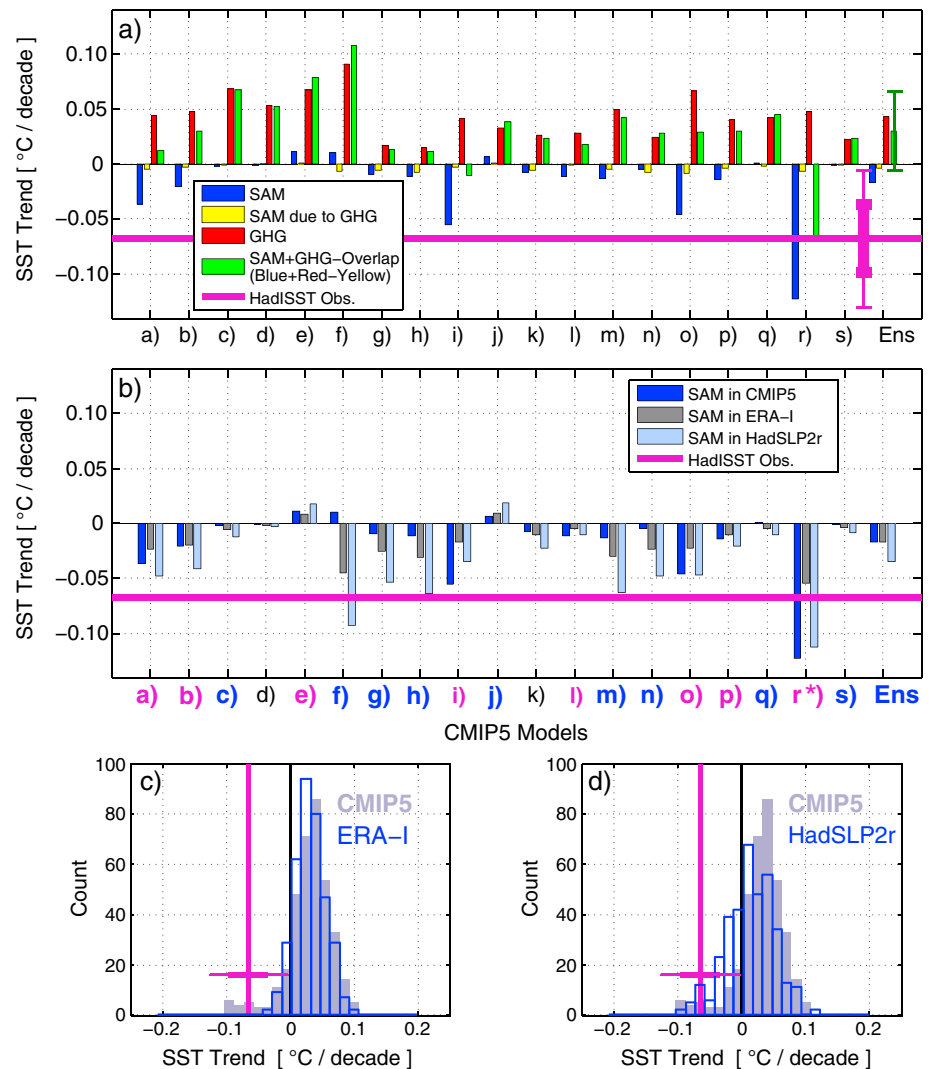


**Figure 4.** (a) Breakdown of contributions to the SO SST reconstructions ( $^{\circ}$  C per decade) in Figure 3a. Blue (red) bars: contribution of December–May SAM (GHG forcing) to the SO SST trend. Yellow bars: the SO SST trend due to a GHG-induced SAM trend. Green bars: full reconstruction. Alphabetical labels match models as in Figure 2. Last entry: ensemble mean (Ens)  $\pm 1$  intermodel standard deviation (ticked vertical green line). The horizontal magenta line denotes the observed SO SST trend ( $^{\circ}$  C per decade) from HadISST. The thick (thin) vertical magenta line shows the one (two)  $\sigma_{\text{RMSE}}$  estimation error on *our own* reconstructions; (b) estimated SAM contribution to the SO SST trend ( $^{\circ}$  C per decade) based on SAM from CMIP5 simulations (dark blue as in Figure 4a), ERA-Interim (dark gray), and HadSLP2r (light blue). Models noticeably overestimating (underestimating) the SAM trend relative to ERA-Interim are marked with magenta (blue) letters. Only MRI-CGCM3 (marked by an asterisk) overestimates the SAM trend relative to HadSLP2r; (c) Shading: distribution of trends obtained by calculating all  $19^2$  possible combinations of the contributions due to SAM and GHG. The vertical magenta line denotes the observed 1979–2014 SO SST trend ( $^{\circ}$  C per decade). The thick (thin) horizontal magenta line shows an expected error margin of one (two)  $\sigma_{\text{RMSE}}$  on *our own* reconstructions. Dark blue contours: distribution of bias-corrected SO SST reconstructions ( $^{\circ}$  C per decade) using seasonal SAM indices from ERA-Interim (Figure 4c) and (d) HadSLP2r. The shaded histograms in Figures 4d and 4c are identical.

in response to a positive SAM trend due to a fast time scale of crossover from cooling to warming (Figure 2a). In addition, CMIP5 models differ among each other in the simulated historical evolution of the SAM itself (Figure 1d). This intermodel spread in the SAM trends also contributes to the large diversity in simulated SO SST responses across the ensemble.

Next, we examine the relationship between the estimated SO SST responses to GHG forcing and the responses to December–May SAM across models. We do not find a significant correlation between the components of the SO SST trend induced by GHG forcing and SAM. We therefore assume that the seasonal SAM contribution

to the SO SST trends is statistically independent of the GHG contribution across the set of models. However, we assume that  $\widehat{SST}_{TrendInter}$  is not independent of  $\widehat{SST}_{TrendSAM}$ .

These assumptions allow us to consider all possible combinations of the CMIP5-based  $\widehat{SST}_{TrendSAM}$ ,  $\widehat{SST}_{TrendGHG}$ , and  $\widehat{SST}_{TrendInter}$  terms. Since our original ensemble contains 19 models, the total number of possible recombinations of  $\widehat{SST}_{TrendSAM}$  and  $\widehat{SST}_{TrendGHG}$  is  $19^2$ . These recombinations give us a wide range of model-based values for the SO SST response  $\widehat{SST}_{TrendAll}$  as represented by the shaded histograms in Figures 4c and 4d.

There is a notable positive bias in the distribution of these synthetic SO SST trends  $\widehat{SST}_{TrendAll}$  relative to observations. Most combinations of model-based  $\widehat{SST}_{TrendSAM}$ ,  $\widehat{SST}_{TrendGHG}$ , and  $\widehat{SST}_{TrendInter}$  produce a net warming. We assume that  $\sigma_{RMSE}$  from our original CMIP5 reconstructions (Figure 3a) is a good estimate for the expected margin of error on  $\widehat{SST}_{TrendAll}$ . Yet, even if we consider this generous margin of error, very few  $\widehat{SST}_{TrendAll}$  combinations fall within  $\pm 1\sigma_{RMSE}$  of the observed SO SST trend. Similar results are obtained with the alternative definition of the SAM index (Figure S6 in the Supporting Information). In the following section, we show that a bias in the historical summer and fall SAM anomalies can potentially prevent the successful simulation of the 1979–2014 SO cooling trends in some models.

### 3.2. Interpretation of CMIP5 Biases Relative to Observations

We now attempt to quantify how biases in the CMIP5 historical SAM (Figure 1c,d) contribute to the discrepancy between simulated and observed 1979–2014 SO SST trends (Figure 1a,b). To answer this question, we extend the above analysis to estimate whether CMIP5 historical experiments would simulate stronger SO cooling, had they represented the seasonal SAM trends realistically. All observationally based SAM indices have sources of uncertainty (Swart et al., 2015). Hence, we consider two data sets that provide different estimates of the observed SAM trend: the gridded HadSLP2r product (Allan & Ansell, 2006) and ERA-Interim reanalysis (Dee et al., 2011). We thus evaluate the bias in CMIP5 historical SAM trends and its impact on SO SST trends. Some models simulate historical SAM trends greater than the one seen in ERA-Interim (Figure 4b, magenta labels), while others underestimate this observationally based trend (Figure 4b, blue labels). In contrast, only one model (MRI-CGCM3) exhibits a historical SAM trend that is stronger than the one seen in HadSLP2r. We convolve the observationally based December–May SAM indices with the model-based SO SST step-response functions. These convolutions allow us to identify models that would simulate enhanced SAM-induced SO cooling, had they reproduced the observed SAM trend. We find that most models would exhibit stronger (weaker) SAM-induced cooling under stronger (weaker) SAM trends (Figures 4b and S7 in the supporting information). However, several models such as CCSM4 are expected to show *stronger SO warming* under a *stronger* positive SAM trend (Figure 4b) because of their fast crossover time scale in Figure 2a. The different behavior of these GCMs may have to do with biases in their climatology of the mean SO thermal stratification that represents the distribution of the background heat reservoir (Ferreira et al., 2015; Holland et al., 2017; Kostov et al., 2017; Schneider & Deser, 2017). Kostov et al. (2017) demonstrate that a large fraction of the intermodel spread in CMIP5 SO SST responses to SAM can be explained in terms of the models' time-mean temperature gradients. Models that quickly transition between a cooling and a warming response to SAM tend to exhibit weak meridional and strong vertical temperature gradients in their SO climatology.

As previously, we compute a range of plausible 1979–2014 SO SST trends that combine GHG and SAM contributions, but this time we use the convolutions of SAM step-response functions with observationally based SAM trends (Figure 4b). We compare the distribution of these bias-corrected SO SST reconstructions (clear histograms, Figures 4c and 4d) against the reconstructions made with the models' own historical SAM trends (shaded histograms, Figures 4c and 4d). The spread in the distribution of synthetic SO SST trends becomes narrower if we use a seasonal SAM index based on ERA-Interim data (Figure 4c and a similar result with the Marshall, 2003, index in Figure S8 of the supporting information). We also find a small but noticeable shift of the distribution toward more negative SO SST trends when we use ERA-Interim SAM to bias-correct the models. Using a SAM index based on the HadSLP2r data set shifts the distribution of synthetic trends even closer to the observed SO SST trend but does not reduce the spread (Figure 4d).

Finally, we examine the subset of combinations in Figures 4c and 4d that reproduce the observed 1979–2014 SO SST trend within the expected margin of error  $\sigma_{RMSE} = 0.031^\circ \text{C}$  per decade. Synthetic combinations in which the step-response function to December–May SAM crosses over to a warming regime in less than  $\sim 15$  years (Figures 2a and 2b) are not able to reproduce the observed SO SST trend within two  $\sigma_{RMSE}$ , regardless of how slowly their SO responds to GHG forcing. The same constraint emerges independent of the

observationally based product (HadSLP2r or ERA-Interim) that we use in our bias correction (Figure 2b). As an exception, the step-response function of model GFDL-ESM2G is able to reproduce significant multidecadal SAM-induced cooling even though it crosses over to a warming regime after  $\sim 10$  years.

We thus suggest that two-time scale step responses to SAM which cross over to a strong warming regime on a short time scale cannot reproduce multidecadal SAM-induced SO cooling. Therefore, such step-response functions are not consistent with our premise, the hypothesis put forward in previous studies (e.g., Purich et al., 2016) that the positive SAM trend is a major driver of the 1979–2014 Southern Ocean cooling. We discuss important implications of this result in section 4.

The step responses to GHG forcing also affect the SO SST reconstruction. Across all models, the SO SST exhibits a warming response to GHG forcing on all time scales. However, models that exhibit weak SO responses to GHG forcing are more likely to simulate historical SO SST cooling induced by the SAM or by a different source of variability (Figure 2d).

#### 4. Discussion and Conclusions

This analysis demonstrates the importance of anthropogenic GHG forcing and the December–May seasonal SAM for contributing to the anomalous 1979–2014 SO SST trends. The response to these two drivers of SO variability explains a large fraction of the intermodel spread across CMIP5 historical simulations, as well as part of the model bias relative to SO SST observations. Our results provide a useful insight into the contributions of GHG forcing and the seasonal SAM to the historical SO SST trends and help identify a combination of model characteristics that favors simulating a 1979–2014 SO cooling similar to the observed SST trend. We show that the trade-off between GHG and SAM-induced SST anomalies is model dependent and governed by several factors.

First, the impact of GHG forcing on SO SST, although unanimously positive, is different in magnitude across the ensemble. All models show an SO SST response under abrupt CO<sub>2</sub> quadrupling that is delayed relative to the response of the global average or the Northern Hemisphere SST (Marshall et al., 2014). These results are consistent with the interhemispheric asymmetry described by Manabe et al. (1990) and reflect the large thermal inertia of the SO (Manabe et al., 1992). However, abrupt CO<sub>2</sub> quadrupling experiments suggest that some models exhibit a more delayed or dampened SO warming response than others. This intermodel diversity is not surprising since CMIP5 ensemble members differ in their seasonal SO mixed layer depth (Salleé, Shuckburgh, Bruneau, Meijers, Bracegirdle, & Wang, 2013), their deep SO convection under GHG forcing (de Lavergne et al., 2014), and the strength of their meridional overturning in the SO (Armour et al., 2016; Downes & Hogg, 2013; Meijers, 2014; Salleé, Shuckburgh, Bruneau, Meijers, Bracegirdle, Wang, & Roy, 2013). These factors affect the mixing and advection of anthropogenic heat that in turn set the time scale of oceanic response to forcing (Stouffer, 2004).

In most CMIP5 models, a positive SAM trend in December–May induces an SO cooling trend that counteracts the warming effect of GHG forcing. However, several models exhibit positive SAM-induced SO SST trends that reinforce the warming due to GHG forcing. The models' inherent response to summer and fall SAM is expected to be different across CMIP5 ensemble members and sensitive to their SO climatology, as discussed in Kostov et al. (2017). Biases in the background meridional and vertical temperature gradients affect the fast and slow responses of SO SST and sea ice to SAM (Ferreira et al., 2015; Holland et al., 2017; Kostov et al., 2017). Our convolutions with SAM integrate both the fast and the slow characteristic responses shown in Figure 2a. For some models, an inherent slow warming regime of the step-response function dominates the SAM convolution on multidecadal time scales. Our results suggest that these particular models cannot simulate a 1979–2014 SAM-induced cooling trend. We furthermore demonstrate that across all models, the seasonal SAM trends in December–May play a greater role in driving the SO SST response than the June–November SAM trends, in agreement with Purich et al. (2016) and consistent with the observed modulation of the SO seasonal sea-ice extent (Doddridge & Marshall, 2017).

Finally, our study points to the central role of accurately simulating the seasonal SAM trends. Models exhibit a large spread in the historical trends of the seasonal SAM indices. A number of models overestimate the observed SAM trend in the summer/fall period. In contrast, the seasonal SAM trend in other historical simulations is more than a factor of two smaller than the corresponding trend in ERA-Interim reanalysis. The mismatch between modeled and observationally based SAM trends is even larger if we use data from

HadSLP2r to define the SAM index. However, the latter result should be approached with caution because of temporal inhomogeneity in HadSLP2r (the data set is extended with NCEP/NCAR reanalysis after 2004). Natural variability in the Southern Hemisphere extratropical atmospheric circulation may explain some of these discrepancies between simulated and observed SAM trends (Thomas et al., 2015).

However, CMIP5 biases may also be related to the models' ability to simulate the dynamical response to stratospheric ozone depletion above Antarctica. The ozone forcing prescribed by the CMIP5 protocol may be another source of bias in the historical simulations. As in observations, the SAM trends in most CMIP5 models are indeed most strongly positive in the austral summer. This seasonal signature is consistent with the impact of the ozone hole that projects onto the SAM pattern in the austral summer and fall (Solomon et al., 2015; Thompson & Solomon, 2002; Thompson et al., 2011). However, Neely et al. (2014) suggest that CMIP5 historical simulations may underestimate the magnitude of ozone depletion because they use monthly mean ozone concentration.

We attempt to account for and correct biases in the models' December-May SAM. Our results suggest that the spread in simulated SO SST trends would be reduced if models matched the 1979–2014 summer and fall SAM trend seen in ERA-Interim data, and there would be a small but noticeable shift in the distribution toward less warming and more cooling. We also attempt to bias-correct the CMIP5 simulations using HadSLP2r as a reference, while acknowledging the aforementioned temporal inhomogeneity in this data set. We find that many CMIP5 models would exhibit stronger cooling or weaker warming SST trends in the SO, had they matched the summer and fall SAM trends in HadSLP2r. On the other hand, our analysis suggests that a handful of CMIP5 models would show a larger SO warming response if they reproduced the strong historical SAM trend of HadSLP2r. Thus, biases in the SAM can explain part of the intermodel spread in SO SST trends and even some of the mismatch between simulated and observed SO SST trends. This result remains valid irrespective of the data set used for bias-correction, ERA-Interim or HadSLP2r. However, after correcting for biases in the historical SAM, our synthetic reconstructions still exhibit a noticeable spread because of the diversity in model-based SO SST step-response functions. Therefore, a substantial fraction of the intermodel differences in the 1979–2014 SO SST trends can be attributed to inherent characteristics of the models as reflected in their step-response functions.

Our study does not take into account other atmospheric modes of variability in addition to the SAM or address the role of freshwater fluxes and SO convection in driving the SST trends. Complications may arise from the fact that the El Niño–Southern Oscillation, a leading global mode of variability, projects on the SAM (Ding et al., 2014; Stuecker et al., 2017) and affects SO SST (Ding et al., 2014; Stuecker et al., 2017; Yuan, 2004). Other factors such as freshwater fluxes (Armour et al., 2016; Pauling et al., 2015) and convective variability (Latif et al., 2013; Seviour et al., 2016, 2017) can drive large multidecadal SO cooling trends. Our response functions implicitly account for freshwater flux anomalies associated with changes in the hydrological cycle induced by GHG forcing and SAM trends. However, our response functions neglect other sources of freshwater forcing such as that from melting land ice (Bintanja et al., 2013; Pauling et al., 2015) and sea-ice dynamics (Haumann et al., 2014). Moreover, our quasi-Green's function analysis does not account for the feedback that air-sea heat flux anomalies (Baker et al., 2017) and sea-ice (Bracegirdle et al., 2018) may exert on the atmospheric circulation and the SAM. These factors contribute to the uncertainty on our SO SST reconstructions.

In our analysis of SO SST trends, we have treated individual models and their step-response functions as independent samples. Yet some GCMs included in CMIP5 share a common genealogy (Knutti et al., 2013). This interdependence may affect the ensemble spread in SO step-response functions, the distribution of historical SO SST trends across CMIP5, and the distribution of our synthetic reconstructions.

Despite these limitations, we have identified a combination of important model characteristics that favor and facilitate the simulation of negative SO SST trends over the 1979–2014 period: a slow SO warming in response to GHG forcing, and a slow transition from strong cooling to warming in response to SAM changes. Assuming that the SAM trend is the primary mechanism responsible for the observed multidecadal SO cooling, we have constrained a joint set of model-based GHG and SAM step-response functions. We cannot judge with certainty if this is the most realistic subset of CMIP5 step-response functions because the observed SO cooling may be due to a physical mechanism unrelated to the SAM and not considered here. However, if the SAM trend has instead induced SO warming, then the mechanism behind the 1979–2014 cooling must have been strong enough to overcome a combination of both SAM and GHG-induced multidecadal warming. What is certain is that the diversity of model SO SST responses to GHG forcing and SAM contributes substantially to individual

model biases and to the intermodel spread in simulated 1979–2014 SO SST trends. Thus, a priority going forward is to understand the causes behind this diversity of model responses to GHG forcing and SAM and to devise relevant observational constraints.

#### Acknowledgments

The CMIP5 data for this study are accessible at the Earth System Grid Federation (ESGF) Portal (<https://esgf-node.llnl.gov/search/cmip5/>). Y. K. was funded by an NSF MOBY grant (NSF OCE-1048926). J. M. and D. F. received support from the NSF FESD Ozone Hole grant (NSF OCE-1338814). J. M. was funded by the NSF grant Dynamics of the Antarctic Seasonal Ice Zone (NSF PLR-1543366). K. C. A. was funded by an NSF grant OCE-1523641. We would like to thank the World Climate Research Programme and the Working Group on Coupled Modeling, which coordinates CMIP5. We extend our appreciation to the organizations in charge of the CMIP infrastructure: the U.S. Department of Energy through its Program for Climate Model Diagnosis and Intercomparison and the Global Organization for Earth System Science Portals. We thank the CMIP5 climate modeling groups for making their numerical output available. We express our gratitude to Susan Solomon for her helpful feedback.

#### References

- Allan, R., & Ansell, T. (2006). A new globally complete monthly historical gridded mean sea level pressure dataset (HadSLP2): 1850–2004. *Journal of Climate*, *19*, 5816–5842. <https://doi.org/10.1175/JCLI3937.1>
- Armour, K. C., & Bitz, C. M. (2015). Observed and projected trends in Antarctic sea ice. *US CLIVAR Variations*, *13*(4), 13–19.
- Armour, K. C., Marshall, J., Scott, J., Donohoe, A., & Newsom, E. R. (2016). Southern Ocean warming delayed by circumpolar upwelling and equatorward transport. *Nature Geoscience*, *9*, 549–555. <https://doi.org/10.1038/ngeo2731>
- Baker, H. S., Woollings, T., & Mbengue, C. (2017). Eddy-driven jet sensitivity to diabatic heating in an idealized GCM. *Journal of Climate*, *30*(16), 6413–6431. <https://doi.org/10.1175/JCLI-D-16-0864.1>
- Bintanja, R., van Oldenborgh, G. J., Drijfhout, S. S., Wouters, B., & Katsman, C. A. (2013). Important role for ocean warming and increased ice-shelf melt in Antarctic sea-ice expansion. *Nature Geoscience*, *6*, 376–379. <https://doi.org/10.1038/ngeo1767>
- Bitz, C. M., & Polvani, L. M. (2012). Antarctic climate response to stratospheric ozone depletion in a fine resolution ocean climate model. *Geophysical Research Letters*, *39*, L20705. <https://doi.org/10.1029/2012GL053393>
- Bracegirdle, T. J., Hyder, P., & Holmes, C. R. (2018). CMIP5 diversity in southern westerly jet projections related to historical sea ice area: strong link to strengthening and weak link to shift. *Journal of Climate*, *31*, 195–211. <https://doi.org/10.1175/JCLI-D-17-0320.1>
- Bracegirdle, T. J., Shuckburgh, E., Sallee, J.-B., Wang, Z., Meijers, A. J. S., Bruneau, N., ... Wilcox, L. J. (2013). Assessment of surface winds over the Atlantic, Indian and Pacific Ocean sectors of the Southern Ocean in CMIP5 models: Historical bias, forcing response and state dependence. *Journal of Geophysical Research: Atmospheres*, *118*, 547–562. <https://doi.org/10.1002/jgrd.50153>
- Ciasto, L. M., & Thompson, D. W. J. (2008). Observations of large scale ocean atmosphere interaction in the Southern Hemisphere. *Journal of Climate*, *21*, 1244–1259. <https://doi.org/10.1175/2007JCLI1809.1>
- de Lavergne, C., Palter, J. B., Galbraith, E. D., Bernardello, R., & Marinov, I. (2014). Cessation of deep convection in the open Southern Ocean under anthropogenic climate change. *Nature Climate Change*, *4*, 278–282. <https://doi.org/10.1038/nclimate2132>
- Dee, D. P., Uppala, S. M., Simmons, A. J., Berrisford, P., Poli, P., Kobayashi, S., ... Vitart, F. (2011). The ERA-Interim reanalysis: Configuration and performance of the data assimilation system. *Quarterly Journal of the Royal Meteorological Society*, *137*, 553–597. <https://doi.org/10.1002/qj.828>
- Ding, H., Greatbatch, R. J., & Gollan, G. (2014). Tropical influence independent of ENSO on the austral summer Southern Annular Mode. *Geophysical Research Letters*, *41*, 3643–3648. <https://doi.org/10.1002/2014GL059987>
- Doddridge, E. W., & Marshall, J. (2017). Modulation of the seasonal cycle of Antarctic sea ice extent related to the Southern Annular Mode. *Geophysical Research Letters*, *44*, 9761–9768. <https://doi.org/10.1002/2017GL074319>
- Downes, S. M., & Hogg, A. M. (2013). Southern Ocean circulation and eddy compensation in CMIP5 models. *Journal of Climate*, *26*(18), 7198–7220. <https://doi.org/10.1175/JCLI-D-12-00504.1>
- Fan, T., Deser, C., & Schneider, D. P. (2014). Recent Antarctic sea ice trends in the context of Southern Ocean surface climate variations since 1950. *Geophysical Research Letters*, *41*, 2419–2426. <https://doi.org/10.1002/2014GL059239>
- Ferreira, D., Marshall, J., Bitz, C. M., Solomon, S., & Plumb, A. (2015). Antarctic ocean and sea ice response to ozone depletion: A two-time-scale problem. *Journal of Climate*, *28*, 1206–1226. <https://doi.org/10.1175/JCLI-D-14-00313.1>
- Fyfe, J. C., Saenko, O. A., Zickfeld, K., Eby, M., & Weaver, A. J. (2007). The role of poleward-intensifying winds on Southern Ocean warming. *Journal of Climate*, *20*, 5391–5400. <https://doi.org/10.1175/2007JCLI1764.1>
- Gillett, N. P., & Thompson, D. W. J. (2003). Simulation of recent Southern Hemisphere climate change. *Science*, *302*, 273–275. <https://doi.org/10.1126/science.1087440>
- Hall, A., & Visbeck, M. (2002). Synchronous variability in the Southern Hemisphere atmosphere, sea ice, and ocean resulting from the Annular Mode\*. *Journal of Climate*, *15*, 3043–3057. [https://doi.org/10.1175/1520-0442\(2002\)015<3043:SWITSH>2.0.CO;2](https://doi.org/10.1175/1520-0442(2002)015<3043:SWITSH>2.0.CO;2)
- Hansen, J., Sato, M., Kharecha, P., & von Schuckmann, K. (2011). Earth's energy imbalance and implications. *Atmospheric Chemistry and Physics*, *11*, 13421–13449. <https://doi.org/10.5194/acp-11-13421-2011>
- Hasselmann, K., Sausen, R., Maier-Reimer, E., & Voss, R. (1993). On the cold start problem in transient simulations with coupled atmosphere-ocean models. *Climate Dynamics*, *9*, 53–61. <https://doi.org/10.1007/BF00210008>
- Haumann, F. A., Notz, D., & Schmidt, H. (2014). Anthropogenic influence on recent circulation-driven Antarctic sea ice changes. *Geophysical Research Letters*, *41*, 8429–8437. <https://doi.org/10.1002/2014GL061659>
- Hofmann, D. J., Butler, J. H., Dlugokencky, E. J., Elkins, J. W., Masarie, K., Montzka, S. A., & Tans, P. (2006). The role of carbon dioxide in climate forcing from 1979–2004. *Tellus*, *58B*, 614–619. <https://doi.org/10.1111/j.1600-0889.2006.00201.x>
- Holland, M., Landrum, L., Kostov, Y., & Marshall, J. (2017). Sensitivity of Antarctic sea ice to SAM-associated wind anomalies in coupled climate models. *Climate Dynamics*, *49*, 1813–1831. <https://doi.org/10.1007/s00382-016-3424-9>
- Jones, J. M., Gille, S. M., Goosse, H., Abram, N. J., Canziani, P. O., Charman, D. J., ... Vance, T. R. (2016). Assessing recent trends in high-latitude Southern Hemisphere surface climate. *Nature Climate Change*, *6*, 917–926. <https://doi.org/10.1038/nclimate3103>
- Knutti, R., Masson, D., & Gettelman, A. (2013). Climate model genealogy: Generation CMIP5 and how we got there. *Geophysical Research Letters*, *40*, 1194–1199. <https://doi.org/10.1002/grl.50256>
- Kostov, Y., Marshall, J., Hausmann, U., Armour, K. C., Ferreira, D., & Holland, M. (2017). Fast and slow responses of Southern Ocean sea surface temperature to SAM in coupled climate models. *Climate Dynamics*, *48*, 1595–1609. <https://doi.org/10.1007/s00382-016-3162-z>
- Kushner, P. J., Held, I. M., & Delworth, T. L. (2001). Southern Hemisphere atmospheric circulation response to global warming. *Journal of Climate*, *14*, 2238–2249. [https://doi.org/10.1175/1520-0442\(2001\)014<0001:SHACRT>2.0.CO;2](https://doi.org/10.1175/1520-0442(2001)014<0001:SHACRT>2.0.CO;2)
- Latif, M., Martin, T., & Park, W. (2013). Cessation of deep convection in the open Southern Ocean under anthropogenic climate change. *Journal of Climate*, *26*, 7767–7782. <https://doi.org/10.1175/JCLI-D-12-00281.1>
- Lee, S., & Feldstein, S. B. (2013). Detecting ozone- and greenhouse gas-driven wind trends with observational data. *Science*, *339*(6119), 563–567. <https://doi.org/10.1126/science.1225154>
- Manabe, S., Spelman, M. J., & Stouffer, R. J. (1990). Transient-response of a global ocean atmosphere model to a doubling of atmospheric carbon-dioxide. *Journal of Physical Oceanography*, *20*(5), 722–749. [https://doi.org/10.1175/1520-0485\(1990\)020<0722:TROAGO>2.0.CO;2](https://doi.org/10.1175/1520-0485(1990)020<0722:TROAGO>2.0.CO;2)

- Manabe, S., Spelman, M. J., & Stouffer, R. J. (1992). Transient responses of a coupled ocean-atmosphere model to gradual changes of atmospheric CO<sub>2</sub>. Part II: Seasonal response. *Journal of Climate*, *5*, 105–126. [https://doi.org/10.1175/1520-0442\(1992\)005<0105:TROACO>2.0.CO;2](https://doi.org/10.1175/1520-0442(1992)005<0105:TROACO>2.0.CO;2)
- Marshall, G. J. (2003). Trends in the Southern Annular Mode from observations and reanalyses. *Journal of Climate*, *16*, 4134–4143. [https://doi.org/10.1175/1520-0442\(2003\)016<4134:TITSAM>2.0.CO;2](https://doi.org/10.1175/1520-0442(2003)016<4134:TITSAM>2.0.CO;2)
- Marshall, J., Armour, K. C., Scott, J. R., Kostov, Y., Hausmann, U., Ferreira, D., ... Bitz, C. M. (2014). The ocean's role in polar climate change: Asymmetric Arctic and Antarctic responses to greenhouse gas and ozone forcing. *Philosophical Transactions of the Royal Society A*, *372*(2014), 20130040. <https://doi.org/10.1098/rsta.2013.0040>
- Marshall, J., Scott, J. R., Armour, K. C., Campin, J.-M., Kelley, M., & Romanou, A. (2015). The ocean's role in the transient response of climate to abrupt greenhouse gas forcing. *Climate Dynamics*, *44*(7), 2287–2299. <https://doi.org/10.1007/s00382-014-2308-0>
- Meijers, A. J. S. (2014). The Southern Ocean in the Coupled Model Intercomparison Project phase 5. *Philosophical Transactions of the Royal Society A*, *372*, 20130296. <https://doi.org/10.1098/rsta.2013.0296>
- Neely, R. R., Marsh, D. R., Smith, K. L., Davis, S. M., & Polvani, L. M. (2014). Biases in Southern Hemisphere climate trends induced by coarsely specifying the temporal resolution of stratospheric ozone. *Geophysical Research Letters*, *41*, 8602–8610. <https://doi.org/10.1002/2014GL061627>
- Oke, P., & England, M. (2004). Oceanic response to changes in the latitude of the Southern Hemisphere subtropical westerly winds. *Journal of Climate*, *17*, 1040–1054. [https://doi.org/10.1175/1520-0442\(2004\)017<1040:ORTCIT>2.0.CO;2](https://doi.org/10.1175/1520-0442(2004)017<1040:ORTCIT>2.0.CO;2)
- Pauling, A. G., Bitz, C. M., Smith, I. J., & Langhorne, P. J. (2015). The Response of the Southern Ocean and Antarctic sea ice to freshwater from ice shelves in an Earth system model. *Journal of Climate*, *29*, 1655–1672. <https://doi.org/10.1175/JCLI-D-15-0501.1>
- Purich, A., Caj, W., England, M. H., & Cowan, T. (2016). Evidence for link between modelled trends in Antarctic sea ice and underestimated westerly wind changes. *Nature Communications*, *7*, 10409. <https://doi.org/10.1038/ncomms10409>
- Rayner, N. A., Parker, D. E., Horton, E. B., Folland, C. K., Alexander, L. V., Rowell, D. P., ... Kaplan, A. (2003). Global analyses of sea surface temperature, sea ice, and night marine air temperature since the late nineteenth century. *Journal of Geophysical Research*, *108*(D14), 4407. <https://doi.org/10.1029/2002JD002670>
- Russell, J. L., Dixon, K. W., Gnanadesikan, A., Stouffer, R. J., & Toggweiler, J. R. (2006). The Southern Hemisphere westerlies in a warming world: Propping open the door to the deep ocean. *Journal of Climate*, *19*, 6382–6390. <https://doi.org/10.1175/JCLI3984.1>
- Salleé, J.-B., Shuckburgh, E., Bruneau, N., Meijers, A. J. S., Bracegirdle, T. J., & Wang, Z. (2013). Assessment of Southern Ocean mixed layer depths in CMIP5 models: Historical bias and forcing response. *Journal of Geophysical Research: Oceans*, *118*, 1845–1862. <https://doi.org/10.1002/jgrc.20157>
- Salleé, J.-B., Shuckburgh, E., Bruneau, N., Meijers, A. J. S., Bracegirdle, T. J., Wang, Z., & Roy, T. (2013). Assessment of Southern Ocean water mass circulation and characteristics in CMIP5 models: Historical bias and forcing response. *Journal of Geophysical Research: Oceans*, *118*, 1830–1844. <https://doi.org/10.1002/jgrc.20135>
- Schneider, D. P., & Deser, C. (2017). Tropically driven and externally forced patterns of Antarctic sea ice change: Reconciling observed and modeled trends. *Climate Dynamics*. <https://doi.org/10.1007/s00382-017-3893-5>
- Sen Gupta, A., Santoso, A., Taschetto, A. S., Ummenhofer, C. C., Trevena, J., & England, M. H. (2009). Projected changes to the Southern Hemisphere ocean and sea ice in the IPCC AR4 climate models. *Journal of Climate*, *22*, 3047–3078. <https://doi.org/10.1175/2008JCLI2827.1>
- Seviour, W. J. M., Gnanadesikan, A., & Waugh, D. W. (2016). The transient response of the southern ocean to stratospheric ozone depletion. *Journal of Climate*, *29*, 7383–7396. <https://doi.org/10.1175/JCLI-D-16-0198.1>
- Seviour, W. J. M., Gnanadesikan, A., Waugh, D., & Pradal, M. A. (2017). Transient response of the Southern Ocean to changing ozone: Regional responses and physical mechanisms. *Journal of Climate*, *30*, 2463–2480. <https://doi.org/10.1175/JCLI-D-16-0474.1>
- Solomon, A., & Polvani, L. M. (2016). Highly significant responses to anthropogenic forcings of the midlatitude jet in the Southern Hemisphere. *Journal of Climate*, *29*, 3463–3470. <https://doi.org/10.1175/JCLI-D-16-0034.1>
- Solomon, A., Polvani, L. M., Smith, K. L., & Abernathy, R. P. (2015). The impact of ozone depleting substances on the circulation, temperature, and salinity of the Southern Ocean: An attribution study with CESM1(WACCM). *Journal of Geophysical Research*, *42*, 5547–5555. <https://doi.org/10.1002/2015GL064744>
- Son, S.-W., Gerber, E. P., Perlwitz, J., Polvani, L. M., Gillett, N. P., Seo, K.-H., ... Yamashita, Y. (2010). Impact of stratospheric ozone on Southern Hemisphere circulation change: A multimodel assessment. *Journal of Geophysical Research*, *115*, D00M07. <https://doi.org/10.1029/2010JD014271>
- Stouffer, R. J. (2004). Time scales of climate response. *Journal of Climate*, *17*, 209–217. [https://doi.org/10.1175/1520-0442\(2004\)017<0209:TSOCR>2.0.CO;2](https://doi.org/10.1175/1520-0442(2004)017<0209:TSOCR>2.0.CO;2)
- Stuecker, M. F., Bitz, C. M., & Armour, K. C. (2017). Conditions leading to the unprecedented low Antarctic sea ice extent during the 2016 austral spring season. *Geophysical Research Letters*, *44*, 9008–9019. <https://doi.org/10.1002/2017GL074691>
- Swart, N., Fyfe, J., Gillett, N., & Marshall, G. J. (2015). Comparing trends in the southern annular mode and surface westerly jet. *Journal of Climate*, *28*, 8840–8859. <https://doi.org/10.1175/JCLI-D-15-0334.1>
- Taylor, K. E., Stouffer, R. J., & Meehl, G. A. (2012). An overview of CMIP5 and the experiment design. *Bulletin of the American Meteorological Society*, *93*, 485–498. <https://doi.org/10.1175/BAMS-D-11-00094.1>
- Thomas, J. L., Waugh, D. W., & Gnanadesikan, A. (2015). Southern Hemisphere extratropical circulation: Recent trends and natural variability. *Geophysical Research Letters*, *42*, 5508–5515. <https://doi.org/10.1002/2015GL064521>
- Thompson, D., & Solomon, S. (2002). Interpretation of recent Southern Hemisphere climate change. *Science*, *296*(5569), 895–899. <https://doi.org/10.1126/science.1069270>
- Thompson, D. W. J., Solomon, S., Kushner, P. J., England, M. H., Grise, K. M., & Karoly, D. J. (2011). Signatures of the Antarctic ozone hole in Southern Hemisphere surface climate change. *Nature Geoscience*, *4*, 741–749. <https://doi.org/10.1038/ngeo1296>
- Wang, G., Cai, W., & Purich, A. (2014). Trends in Southern Hemisphere wind-driven circulation in CMIP5 models over the 21st century: Ozone recovery versus greenhouse forcing. *Journal of Geophysical Research: Oceans*, *119*, 2974–2986. <https://doi.org/10.1002/2013JC009589>
- Xie, S.-P., Lu, B., & Xiang, B. (2013). Similar spatial patterns of climate response to aerosol and greenhouse gas changes. *Nature Geoscience*, *6*, 828–832. <https://doi.org/10.1038/NGEO1931>
- Yeo, S.-R., & Kim, K.-Y. (2015). Decadal changes in the Southern Hemisphere sea surface temperature in association with El Niño–Southern Oscillation and Southern Annular Mode. *Climate Dynamics*, *45*(11–12), 3227–3242. <https://doi.org/10.1007/s00382-015-2535-z>
- Yuan, X. J. (2004). ENSO-related impacts on Antarctic sea ice: A synthesis of phenomenon and mechanisms. *Antarctic Science*, *16*(4), 415–425. <https://doi.org/10.1017/S0954102004002238>